Reliability Assessment of Bridges During Flood Events

Fatemeh Fadaei[1[0009-0004-6582-4788]], Pier Francesco Giordano[1[0000-0003-0396-0253]], Maria Pina Limongelli[1[0000-0002-9353-5439]] and Sebastian Thöns[2[0000-0002-7714-3312]]

[1] Politecnico di Milano, Via Giuseppe Ponzio 31, 20133 Milan, Italy
[2] BAM Federal Institute for Materials Research and Testing, Unter den Eichen 87, 12205 Berlin, Germany
fateme.fadaei@polimi.it

Abstract. Effective bridge management during and after catastrophic events requires balancing user safety with service continuity. This objective can be supported through reliability assessments that leverage real-time Structural Health Monitoring data, enabling informed decision-making under evolving conditions. The need for such an approach is particularly critical during floods, as statistical analyses of bridge failures worldwide identify hydraulic actions as the predominant cause of collapse. Although foundation scour remains the primary cause of failure in watercourse-spanning bridges, a comprehensive reliability assessment must also account for other hydraulic stressors, including hydrodynamic drag forces. This study introduces a reliability assessment framework for bridges subjected to floods, accounting for the combined influence of these hydraulic mechanisms. The framework integrates data from in-situ monitoring systems that continuously measure key structural and hydraulic parameters, allowing the bridge's reliability to be dynamically updated. The proposed approach is demonstrated through a case study, highlighting its applicability and potential to enhance flood risk reduction in bridge management.

Keywords: First Keyword, Second Keyword, Third Keyword.

1 Introduction

Bridges are key components of transportation networks. When a bridge becomes non-functional or collapses, it can cause substantial direct economic losses and severely disrupt transportation networks. Such disruptions affect traffic operations, force vehicles to use longer detour routes, and generate significant costs for repair and reconstruction [1].

Global data indicate that natural hazards are the primary drivers of bridge collapses, with flooding and scour responsible for most of the documented cases [2]. Evidence from past events in Europe illustrates the scale of these impacts. For instance, the 2002 flood in Germany led to approximately €577 million in repair works on bridges and road infrastructure, while flooding in Austria faced the national railway operator in Austria with losses of around €100 million in a few years [3][4]. In the United

Kingdom, the partial or complete destruction of bridges during flood events in 2009 has been estimated to cause economic losses of about £2 million per week [5].

Major flood events typically trigger both types of bridge-related scour—contraction scour and local scour—with local scour recognized as the primary cause of failures occurring at bridge piers [6][7]. This occurs when the scour depth increases significantly, undermining the bridge foundation and reducing its load-bearing capacity, which can lead to structural instability and, ultimately, catastrophic failure [8]. To effectively address this issue and conduct reliability analysis and risk assessment, it is essential to first have an accurate estimation of the scour depth around bridge pier foundations during flood events. Once this estimation is obtained, potential failure mechanisms associated with scour must be further examined and evaluated.

Over the past decades, numerous models have been developed to estimate local scour depth at bridge foundations, including empirical, numerical, and data-driven models [9][10][11][12][13]. Among these, empirical models remain the most widely used in engineering practice. However, most of these formulations are derived from laboratory experiments conducted under simplified and highly controlled conditions, which may not adequately represent the complexity of full-scale field environments. To ensure conservative design, many empirical equations are based on envelope-curve fitting techniques that intentionally overpredict scour depth [3]. This is evident when predicted scour depths using these models are compared with values observed in the field [14]. While these models enhances safety, it also introduces significant epistemic uncertainty into scour predictions. Probabilistic frameworks have been presented over the years to incorporate the effect of these uncertainties [6][15].

In this context, bridge scour monitoring can be implemented as an important complementary approach. Over the years, various types of instrumentation have been developed to measure scour depth at bridge foundations in real time, including single-use devices, pulse or radar sensors, buried or driven rod systems, sound-wave devices, fiber-Bragg grating sensors, and electrical conductivity devices [16]. The data obtained from these monitoring systems can significantly reduce uncertainty in scour estimation. In particular, monitoring observations can be integrated into probabilistic frameworks to update scour predictions at unmonitored locations and provide valuable field evidence to refine existing empirical models [17][18].

Accurately estimating scour depth at bridge foundations is only one component of the overall reliability and risk assessment of bridges subjected to flooding. Equally important—yet considerably more challenging—is predicting the mechanical consequences that scour may impose on the bridge structure. Analyses of historical cases of hydraulically induced bridge failures have identified several possible failure modes, including vertical failure, lateral failure, torsional failure, and bridge deck failure. Among these, most documented cases are associated with lateral failure [7]. Although several studies have numerically investigated the structural behavior of scoured bridges under vertical and lateral loading and have identified potential failure mechanisms, relatively few studies have examined these mechanisms within a probabilistic modeling framework [8][19][20][21][22]. For a comprehensive reliability analysis of bridges subjected to flood-induced scour, it is essential to recognize that soil properties, foundation characteristics, and load systems all involve varying degrees of uncertainty [23].

Uncertainties in soil properties may arise from limited site investigations, insufficient laboratory testing, and inaccuracies in empirical equations used to correlate soil parameters. Uncertainties in foundation properties may be related to geometric or material characteristics of the foundation, as well as the group behavior and performance of piles. Similarly, uncertainties in load systems occur due to different assumptions made in determining load models acting on the foundation [24][25]. Because of these multiple sources of uncertainty affecting both the demand and capacity models, adopting a probabilistic approach in foundation behavior analysis is a logical and necessary step for the bridge reliability assessment.

To address the limitations discussed above, this study proposes an integrated probabilistic framework that links informed scour assessment with the reliability analysis of bridge foundations exposed to flood-induced scour. The framework first estimates local scour depth at complex bridge pier systems composed of a pier stem, pile cap, and pile group. Unlike conventional probabilistic scour assessment approaches, which primarily account for uncertainties in model parameters and input variables, the proposed framework additionally incorporates real-time scour depth observations obtained from monitoring systems. These observations incorporated using a probabilistic updating scheme based on Gaussian Bayesian Networks (GBNs), enabling the initially predicted scour depth at unmonitored locations to be continuously updated as monitoring data become available.

Building on the updated scour estimates, the study subsequently performs a probabilistic reliability analysis of the bridge foundation system under different flood intensities. Two critical scour-related failure mechanisms are considered: (i) the loss of vertical bearing capacity of the pile group and (ii) the loss of lateral load-carrying capacity of the pile group, which is frequently associated with hydraulically induced bridge failures. The analysis incorporates uncertainties affecting both the demand and capacity models, including uncertainties in soil properties, foundation characteristics, and load representations. By coupling real-time scour monitoring, probabilistic scour prediction, and structural reliability assessment within a unified framework, the study provides a more comprehensive methodology for evaluating the safety of bridge foundations under flood conditions and for supporting risk-informed bridge management decisions.

The remainder of this paper is structured as follows. Section 2 presents the methodology, including a brief overview of scour assessment for complex pier systems, the probabilistic framework based on Gaussian Bayesian Networks for updating scour depth using monitoring data, and the reliability analysis, with emphasis on actions and loads on the piers, the considered failure mechanisms, and the formulation of performance functions and system failure modeling. Section 3 introduces the case study used to demonstrate the proposed framework. Section 4 presents and discusses the results and their implications. Finally, Section 5 summarizes the main findings and conclusions of the study.

2 Methodology

2.1 Scour Assessment

Scour Assessment for Complex Piers. Scour at bridge foundations is commonly evaluated using the procedures outlined in the Federal Highway Administration's Hydraulic Engineering Circular No. 18 (HEC-18) [9]. HEC-18 recommends a pier-scour equation for estimating the design scour depth under both live-bed and clear-water conditions:

$$\frac{y_{s,pier}}{y_1} = 2.0k_1k_2k_3\left(\frac{a_{pier}}{y_1}\right)^{0.65}Fr_1^{0.43} \tag{1}$$

where $y_{s,pier}$ is the local scour depth at the pier (m), y_1 is the flow depth upstream of the pier (m), and a_{pier} is the pier width (m). The coefficients k_1, k_2 and k_3 are correction factors accounting for pier nose shape, flow angle of attack, and bed conditions, respectively. Fr_1 is the Froude number defined as $Fr_1=\frac{v_1}{\sqrt{gry_1}}$, where v_1 is the flow velocity upstream of the pier (m/s) and gr is the gravitational acceleration. For simplicity, the relationships between the upstream flow depth y_1 and the discharge q, as well as between velocity and flow depth, can be approximated using Manning's equation for a rectangular channel:

$$y_u = \left(\frac{qn}{bs^{\frac{1}{2}}}\right)^{\frac{3}{5}} \tag{2}$$

$$v_u = \frac{q}{by_u} \tag{3}$$

where q is the flow discharge ($^{m^3}/_{s}$), b is the average channel width (m), n is Manning's coefficient, and s is the channel slope.

In practice, the flow may be obstructed by several substructural components that contribute to scour development. These scour-producing elements typically include the pier stem, the pile cap, and the pile group. Equation (1) implicitly assumes a simplified foundation system consisting of a single pier extending through the soil, such that the calculated pier scour represents the total foundation scour. However, in many bridge foundations each structural component contributes independently to the overall scour depth.

To account for these effects, the scour produced by each component can be estimated using modified forms of the basic pier-scour equation. This is accomplished by representing irregular foundation elements with an equivalent full-depth pier width and by adjusting the flow depth, velocity, and elevation of the element relative to the bed. The scour depths associated with the pile cap and pile group are calculated as:

$$\frac{y_{s,pc}}{y_2} = 2.0k_1k_2k_3k_w\left(\frac{a_{pc}^*}{y_2}\right)^{0.65}\left(\frac{v_2}{\sqrt{gry_2}}\right)^{0.43} \tag{4}$$

$$\frac{y_{s,pg}}{y_3} = k_{h,pg}\left[2.0k_1k_3\left(\frac{a^*_{pg}}{y_3}\right)^{0.65}\left(\frac{v_3}{\sqrt{gry_3}}\right)^{0.43}\right] \tag{5}$$

where $y_{s,pc}$ and $y_{s,pg}$ denote the scour depths associated with the pile cap and pile group, respectively. The variables y_2 and y_3 represent the adjusted flow depths used in the pile-cap and pile-group scour calculations, while v_2 and v_3 are the corresponding adjusted velocities. The parameters a^*_{pc} and a^*_{pg} are the equivalent full-depth solid-pier widths for the pile cap and pile group, respectively. k_w is the wide-pier correction factor and $k_{h,pg}$ is the pile-group height factor. Equation (4) is applicable when the bottom of the pile cap is located above the channel bed and therefore directly exposed to the flow. The total scour depth at the foundation can then be estimated by superimposing the contributions from each component.

In the HEC-18 methodology, the variables in Equation (1) are treated deterministically. As a result, the equation does not explicitly account for uncertainties associated with the model formulation, parameter values, or hydraulic and hydrologic inputs. Any implicit safety margin is embedded within the empirical coefficient 2.0 or within the correction factors k_i [26]. To incorporate these uncertainties in a probabilistic framework, Monte Carlo simulation can be applied. In this approach, random samples of the parameters in Equation (1) to (5) are generated according to specified probability distributions characterized by their statistical moments. Additionally, the scour equation may be modified by introducing a model correction factor to explicitly account for model uncertainty:

$$y_{s,t} = \lambda_{y_s}(y_{s,pier} + y_{s,pc} + y_{s,pg}) \tag{6}$$

GBNs for Inference. Gaussian Bayesian Networks (GBNs) are used for inference by exploiting the correlation among scour depths at different bridge piers. The main idea is that scour depth measurements obtained from sensors installed at a single bridge pier can be extended to unmonitored piers, since the piers are exposed to the same hydraulic conditions and often have similar structural configurations.

Specifically, direct observations of the total scour depth $y_{s,t}$ at the instrumented pier are used to update the moments of the probability density function (pdf) of the model correction factor, λ_{y_s}. The updated distribution of this correction factor is then used to estimate the scour depth at unmonitored piers. In Figure 1, the graphical representation of the GBN for the inference problem is presented.

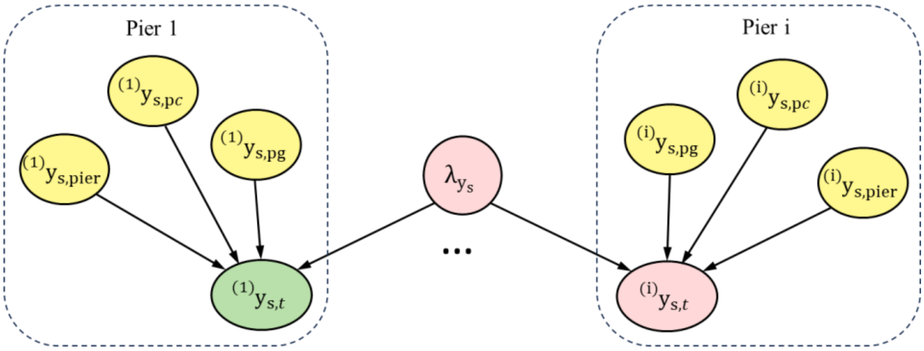

Figure 1. Graphical representation of the GBN for the inference of the scour depth model correction factor

Details on the formulation of the inference problem for the GBN model are provided in [27]. To apply the closed-form solution for inference, several requirements must be satisfied to ensure compatibility with the assumptions of a Gaussian Bayesian Network (GBN). These include:

- (Hp1) all random variables (RVs) must be continuous;
- (Hp2) the RVs must follow a normal/lognormal distribution;
- (Hp3) the relationships between RVs must be linear.

These assumptions enable a complete analytical treatment of the inference problem. In this study, the input variables are assumed to follow either normal or lognormal distributions, which satisfy the requirements of Gaussian Bayesian Networks (GBNs) and are consistent with commonly adopted pdfs in the literature. Under these conditions, the scour assessment problem can be formulated within a GBN framework.

2.2 Reliability Analysis

Actions and Environmental loads. According to the JCSS Probabilistic Model Code [24], the environmental conditions in which structural systems operate generate internal forces, deformations, material deterioration, and other short- or long-term effects. The causes of these effects are referred to as actions, defined as assemblies of concentrated or distributed forces acting on a structure.

The description of an action involves two aspects: physical and statistical. The physical description specifies the characteristics of the load, such as its magnitude, direction, and spatial distribution (e.g., vertical forces distributed over a defined area). The statistical description characterizes the uncertainty associated with the action through probabilistic models, typically expressed by probability density functions.

For a reliable assessment of bridge performance during flood events, all relevant actions acting simultaneously on the structure must be considered, with both their physical representation and statistical characterization incorporated into the analysis. In the present study, the considered actions include the permanent load due to the self-weight of the structure and the variable load associated with traffic in the vertical direction. In the transverse direction, the bridge is subjected to hydrodynamic forces generated by flood flow acting on the submerged portions of the pier, pile cap, and piles. When scour develops, additional hydrodynamic forces may act on newly exposed structural segments where the surrounding soil has been eroded.

Permanent Loads (Self-weight). According to the JCSS Probabilistic Model Code [24], self-weight is classified as a permanent action, characterized by a probability of occurrence that is essentially equal to unity at any given time, negligible temporal variability, and relatively small uncertainty compared with other load types.

Within this framework, the self-weight w of a structural component can be expressed as the integral of the material weight density over the component volume:

$$\mathrm{w} = \int_{\mathrm{vol}} \gamma \,\mathrm{dvol} \tag{7}$$

where vol represents the volume of the structural component, which may vary due to deviations from nominal geometric values, and γ denotes the weight density of the material, treated as a random field.

For structural components whose material properties can reasonably be assumed homogeneous, Equation (7) can be simplified to:

$$\mathrm{w} = \gamma_{\mathrm{ave}}\mathrm{vol} \tag{8}$$

where γ_{ave} is the average weight density of the component. Geometric dimensions such as thickness and width are modeled as:

$$\mathrm{d} = \mathrm{d}_{\mathrm{nom}} + \delta_{\mathrm{d}} \tag{9}$$

where d_{nom} is the nominal dimension specified in the design drawings and δ_d represents the deviation from this nominal value. The deviation δ_d is assumed to follow a Gaussian distribution with mean μ_{δ_d} and standard deviation σ_{δ_d}, implying that the dimension d is also normally distributed. The statistical parameters of δ_d depend on the material type and the structural member considered, and recommended values are provided in the JCSS Probabilistic Model Code [24] and related literature [25].

Traffic. The JCSS Probabilistic Model Code classifies variable actions as loads that exhibit significant temporal fluctuations over time [24]. In fib Bulletin 80 [28], a variable load is modeled by two components: a time-variant component, representing the stochastic fluctuations of the load over time, and a time-invariant component, which accounts for modeling uncertainties associated with the selected load model.

Under this modeling, the maximum value of the variable load over a specified reference period can be expressed as the product of these two components. The bulletin provides example probabilistic models for several categories of variable actions, including traffic loads.

Furthermore, it is emphasized that for reliability verification purposes, the probabilistic distribution used to describe load maxima should correspond to the same reference period adopted in the reliability analysis, ensuring consistency between the statistical characterization of the load effects and the target reliability index.

Hydrodynamic Loads. Hydrodynamic forces arise from the drag generated by the interaction between flowing water and structural elements. These forces typically act on bridge piers and their components when river flow impinges on their exposed surfaces. To evaluate these forces, the formulation provided in Eurocode 1 (EN 1991-1-6) for actions induced by water currents on immersed structures is adopted [29].

According to this model, the total horizontal force f_{wa} exerted by currents on a vertical surface is given by:

$$f_{wa} = \frac{1}{2} c_D \gamma_{wa} y_{wa} b_{comp} v_{wa}^2 \tag{10}$$

where c_D is the drag coefficient, v_{wa} is the mean water velocity averaged over the flow depth, γ_w is the density of water, y_w is the water depth, and b_{comp} is the characteristic width of the structural component exposed to the flow. In the present study, b_{comp} corresponds to the width of the pier stem, pile cap, or piles.

To account for the uncertainties associated with the parameters in Equation (10), a probabilistic framework based on Monte Carlo simulation is employed. In this approach, random samples of the governing parameters are generated according to predefined probability distributions characterized by their statistical moments, allowing the uncertainties of the input variables of the hydrodynamic force model to be captured.

The flow velocity along the height of the pier/pile cap/piles is assumed to follow a uniform vertical profile**.** In the presence of local scour, however, the velocity distribution within the scour hole is approximated as decreasing linearly with depth, reaching zero at a depth equal to one pile diameter below the reference bed level [2].

Failure Mechanisms. Piles serve multiple functions in bridge foundations, including providing additional structural safety beneath abutments and piers, particularly in locations where scour may significantly reduce foundation stability [30]. Bridge scour is a complex phenomenon resulting from the interaction between flowing water, soil, and structural components. Consequently, scour-induced bridge failures involve coupled hydraulic, geotechnical, and structural processes [7].

In this study, two potential failure mechanisms are considered: a geotechnical failure associated with the loss of pile group bearing capacity, and a combined geotechnical–structural failure related to the insufficient lateral capacity of the pile group. These mechanisms are described in the following sections.

Loss of Bearing Capacity of the Pile Group. Here it is assumed that the load transfer in piles occur as a combination of frictional resistance along the pile shaft and end bearing at the pile tip which corresponds to the usual load transfer for most piles, except for the cases where the pile penetrates very soft soil and bears directly on a firm stratum, or where the pile functions primarily as a friction pile.

According to API RP 2A-WSD [31], the ultimate bearing capacity of a pile $q_{ult,i}$ can be expressed as the sum of the contributions from shaft friction and end bearing, both of which depend on the scour depth:

$$q_{\text{ult,i}} = q_{\text{friction,i}} + q_{\text{end bearing,i}} \tag{11}$$

The shaft friction resistance is given by:

$$q_{\text{friction,i}} = q_{\text{u,friction}} a_{\text{s}} \tag{12}$$

and the end bearing resistance is:

$$q_{\text{end bearing,i}} = q_{\text{u,end bearing}} a_{\text{b}} \tag{13}$$

where $q_{\text{u, friction}}$ is the unit shaft friction capacity, a_s is the pile side surface area contributing to friction resistance, q is the unit end bearing capacity, and a_b is the gross base area of the pile.

For piles embedded in cohesionless soils, the unit end bearing capacity can be calculated as:

$$q_{\text{u,end bearing}} = n_{\text{q}} p'_{\text{o}} \tag{14}$$

where n_q is the dimensionless bearing capacity factor and p'_o is the effective overburden pressure (vertical effective stress) at the pile tip depth. This stress depends on the remaining pile penetration depth after accounting for scour. The effective overburden pressure is given by:

$$p'_{\text{o}} = \gamma' z \tag{15}$$

where z is the pile penetration depth and γ' is the effective unit weight of the soil. The unit shaft friction at a given depth may be estimated as:

$$q_{\text{u,friction}} = k_{\text{o}} \tan(\delta) \overline{p'_{\text{o}}} \tag{16}$$

where k_o is the coefficient of lateral earth pressure, δ is the interface friction angle between the soil and the pile, and $\bar{p'_o}(y_s)$ is the average effective overburden pressure, evaluated at the midpoint of the remaining pile penetration depth.

When piles are installed in groups, interaction effects between individual piles can significantly influence the overall foundation capacity. In the case where piles are placed in close proximity, the stress zones associated with shaft friction and end bearing may overlap. If these stresses become sufficiently large, the surrounding soil may undergo shear failure or experience excessive settlement. According to API RP 2A-WSD

[31], group effects should generally be considered when the pile spacing is less than eight pile diameters.

For piles embedded in sandy soils and subjected to axial loading, the group capacity may, in some cases, exceed the sum of the capacities of individual isolated piles due to soil confinement effects. In this study, pile interaction is accounted for through the pile-group efficiency factor $\lambda^{(q_{pile\text{-}group})}$.

The ultimate bearing capacity of the pile group can be estimated by summing the individual pile capacities while accounting for group interaction effects:

$$q_{\text{pile-group}} = \lambda^{(q_{\text{pile-group}})} \sum_{i=1}^{n_{\text{piles}}} q_{\text{ult},i} \tag{17}$$

where n_{piles} is the number of piles in the group.

Loss of Lateral Capacity. For piles embedded in cohesionless soils, the ultimate lateral resistance of laterally loaded piles is governed either by the lateral resistance of the surrounding soil or by the yield or ultimate bending resistance of the pile section. Consequently, failure may occur when the maximum bending moment in the pile reaches the yield resistance of the pile section or when the mobilized lateral earth pressure reaches the ultimate passive resistance of the soil along the embedded pile length [32][2].

Following the classical solutions for laterally loaded piles proposed by Bengt H. Broms [32], piles can be categorized into short, intermediate, and long piles, depending on their embedded length and structural stiffness. For piles fixed against rotation at the head, each category is associated with a different governing failure mechanism.

For short piles, failure occurs through horizontal translation of the pile within the soil mass, with the ultimate passive soil resistance mobilized along the entire embedded length. In this case, failure occurs when the applied lateral load equals the ultimate lateral resistance of the soil:

$$h_{\text{ult}} = 1.5\gamma_{\text{soil}} a_{\text{proj}} l^2 k_p \tag{18}$$

where l is the embedded pile length, γ_{soil} is the unit weight of the soil, a_{proj} is the projected area of the pile per unit depth, and k_p is the coefficient of passive earth pressure. The coefficient k_p can be expressed as a function of the soil internal friction angle φ:

$$k_p = \tan^2\left(45 + \frac{\varphi}{2}\right) \tag{19}$$

As the embedded length increases, a transition regime may occur in which the maximum negative bending moment at the pile head reaches the yield resistance of the pile section. In this case, the ultimate lateral resistance is determined assuming that the lateral earth pressure increases linearly with depth. The ultimate lateral load can then be obtained from equilibrium considerations about the toe of the loaded pile:

$$h_{ult} = \frac{0.5\gamma_{soil} a_{proj} l^3 k_p + M_y}{(l + e)} \tag{20}$$

where e is the eccentricity of the applied lateral load and M_y is the yield moment capacity of the pile section.

For long piles, as illustrated in Figure 2, failure occurs through the formation of a plastic mechanism characterized by the development of two plastic hinges. One hinge forms at the pile head where the maximum negative bending moment reaches the yield resistance, while the second hinge forms at a depth d below the ground surface where the maximum positive bending moment reaches the yield resistance of the pile section.

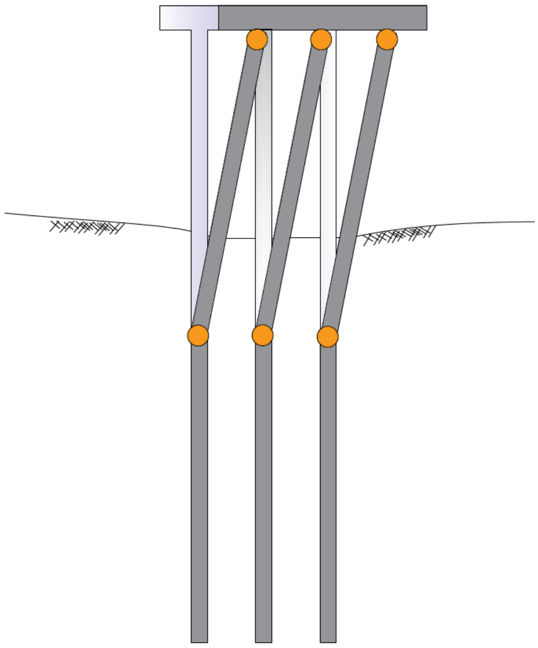

Figure 2. Failure mechanism for long laterally loaded piles

The depth of the plastic hinge can be determined from the condition that the total shear force at this location is equal to zero, assuming that full passive soil resistance develops above that point:

$$d_{hinge}=0.82\sqrt{\frac{h_{ult}}{\gamma a_{pile} k_p}} \tag{21}$$

The ultimate lateral resistance can then be expressed as:

$$h_{ult} = \frac{M_y^+ + M_y^-}{e + 0.544\left(\frac{h_{ult}}{\gamma_{soil} a_{proj} k_p}\right)^{0.5}} \tag{22}$$

At failure, the full passive resistance of the soil develops from the ground surface down to the depth of the plastic hinge, while the soil resistance below this depth may not be fully mobilized.

When piles are installed in groups, interaction between adjacent piles affects the lateral response of the foundation. Similar to the bearing capacity evaluation, the ultimate lateral capacity of a pile group can be estimated as the sum of the individual pile capacities, adjusted by a pile-group efficiency factor, $\lambda^{(h_{pile\text{-}group})}$:

$$h_{pile-group} = \lambda^{(h_{pile-group})} \sum_{i=1}^{n_{piles}} h_{ult,i} \tag{23}$$

For piles with identical head fixity conditions embedded in cohesive or cohesionless soils, pile groups typically exhibit larger lateral deflections and lower lateral resistance compared with a single isolated pile subjected to the same average load. This reduction in resistance is represented in the efficiency factor $\lambda^{(h_{pile\text{-}group})}$.

Performance Functions. The performance of each component of a system can be described using a performance function, also referred to as a limit state function. Failure of a component occurs when the value of the limit state function falls below a specified threshold. In reliability analysis, this condition corresponds to the demand exceeding the capacity of the component.

In this study, the system corresponds to the bridge, while the components correspond to the bridge piers. The probability of failure of component i associated with failure mechanism j is defined as:

$$P_{i,j}(F) = P[g_j(D_{i,j}, C_{i,j}) \leq 0] \tag{24}$$

where $g_j(\cdot)$ is the j-th limit state function, $D_{i,j}$ represents the structural demand, and $C_{i,j}$ denotes the corresponding capacity of component i for failure mechanism j.

In the present study, two failure mechanisms are considered. For the first failure mechanism, failure occurs when the axial load acting on the pile group exceeds its axial bearing capacity. The corresponding limit state function can be written as:

$$g_{1,i} = q_{pile-group,i} - s_{axial,i} \tag{25}$$

where $s_{\text{axial},i}$ is the total axial demand on component i, consisting of the self-weight of the structure and the traffic load, and $q_{\text{pile-group},i}$ is the ultimate bearing capacity of the pile group. For the second failure mechanism the limit state function is defined as:

$$g_{2,i} = h_{pile-group,i} - s_{lateral,i} \tag{26}$$

where $s_{\text{lateral},i}$ represents the total lateral load acting on component i, and $h_{\text{pile-group,i}}$ is the ultimate lateral capacity of the pile group.

System Reliability. The performance of a structural system depends on the states of its individual components. In this study, the bridge is modeled as a series system, meaning that it is a system without any redundancy and the failure of any single component, due to any failure mechanism, leads to failure of the entire system. Such systems are often referred to as weakest-link systems.

Assuming statistical independence between component failures, the system probability of failure is given by:

$$P_{system}(F) = 1 - \prod_{i=1}^{n}(1 - P_i(F)) \tag{27}$$

where n is the number of components and $P_i(F)$ is the probability of failure of component i.

Each component may fail through multiple failure mechanisms. Assuming independence between the failure mechanisms, the probability of failure of component i can be expressed as:

$$P_i(F) = 1 - \prod_{j=1}^{m}(1 - P_{i,j}(F)) \tag{28}$$

where m is the number of failure mechanisms and $P_{i,j}(F)$ is the probability of failure of component i associated with failure mechanism j.

3 Case Study

The study focuses on the piers supporting one of the main spans of a highway viaduct along the A21 Piacenza–Brescia corridor in northern Italy. The viaduct, constructed in 1968, consists of 41 spans with a total length of 1673.5 m and adopts a conventional Gerber structural system with continuous prestressed concrete beams and suspended spans connected through hinges.

Seven spans (spans 30–36) cross the Po River, where the piers are exposed to hydraulic actions and potential scour. Among these, span 32 is selected as a representative case to demonstrate the adopted methodology. It should be noted that, for a comprehensive reliability assessment under flood conditions, all river-crossing piers should ultimately be considered.

The analyzed span has a length of 83 m and is supported by cast-in-place piers founded on deep pile groups (Figure 3). Each pier transfers loads through a pile cap to a group of ten piles arranged in a regular layout, extending to significant depth to ensure adequate foundation stability.

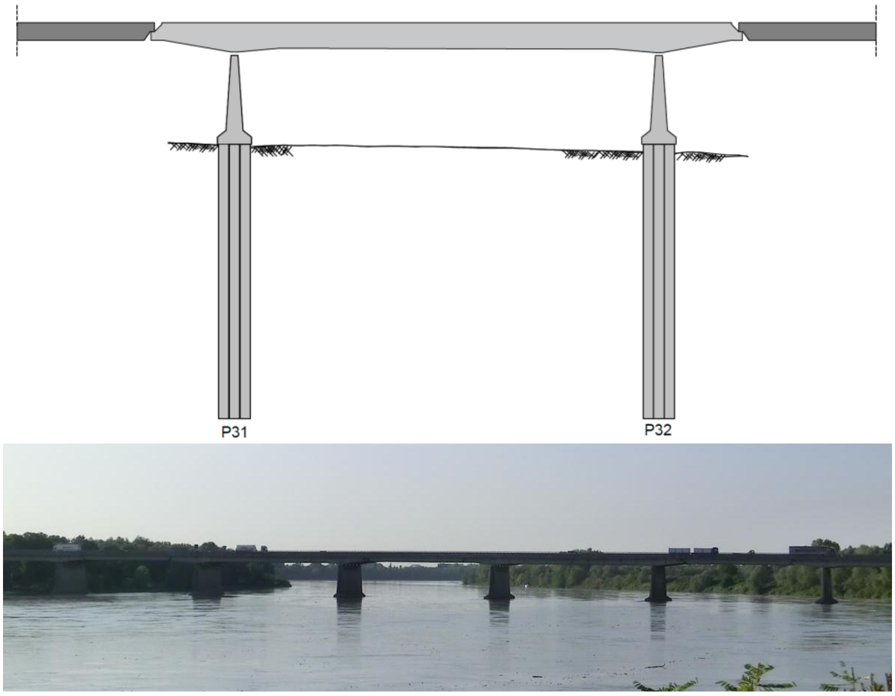

Figure 3. The A21 highway viaduct crossing Po River plus the scheme of the studied main span

Flooding of the Po River is primarily driven by prolonged rainfall events rather than short-duration, high-intensity storms. The hydrological regime is characterized by two flood seasons, typically occurring in late spring (June) and autumn (November), and two low-flow periods in winter (January) and summer (August). Representative discharge statistics indicate an annual maximum flow of approximately 8,000 m³/s with a 10-year return period, and about 12,000 m³/s associated with a return period slightly exceeding 100 years [33].

Tables 1 to 3 present the input variables used for probabilistic modeling of scour depth, as well as load and resistance modeling. Each variable is described by its characteristics, including whether it is stochastic or deterministic, along with its corresponding statistical moments. It should be noted that stochastic variables are denoted by uppercase letters to align with the conventional representation of random variables, while deterministic variables are written in lowercase. Variables referenced in the methodology equations but not listed in the tables are derived variables, computed from the given input variables using the specified equations.

Table 1. Input variables for probabilistic modeling of scour depth.

Var.	Description	Unit	Dist.	Mean	Standard Deviation	Reference
B	River Width	m	Lognormal	420	0.05 * Mean	Assumed
S	River Slope	-	Lognormal	0.002	0.05 * Mean	Assumed
N	Manning's coefficient	-	Lognormal	0.025	0.28 * Mean	[26]
ε_{y_1}	Manning model error term	m	Lognormal	0	0.15	[17]
gr	Acceleration of gravity	m^2/s	Det.	9.81	-	-
$k_{1,pier}$	Correction factor for pier nose shape	-	Det.	0.9	-	[9]
$k_{1,pc}$	Correction factor for pile cap nose shape	-	Det.	0.9	-	[9]
$k_{1,pg}$	Correction factor for pile group nose shape	-	Det.	1	-	[9]
k_2	Correction factor for angle of attack of flow	-	Det.	1	-	[9], [22]
K_3	Correction factor for bed condition	-	Normal	1.1	0.05 * Mean	[26]
A_{pier}	Pier stem width	m	Lognormal	1.75	0.05 * Mean	Assumed
A_{pc}	Pile cap width	m	Lognormal	3.75	0.05 * Mean	Assumed
T_{pc}	Thickness of pile cap	m	Lognormal	2	0.05 * Mean	Assumed

A_{pile}	Pile width	m	Lognormal	1.5	0.05 * Mean	Assumed
s_{pile}	Spacing between piles	m	Det.	1.55	-	-
Λ_{y_s}	Correction factor for scour model	-	Normal	0.55	0.52 * Mean	[26]

Table 2. Input variables for probabilistic modeling of the loads.

Var.	Description	Unit	Dist.	Mean	Standard Deviation	Reference
Γ_{RC}	Reinforced concrete density	kg/m^3	Normal	2500	0.04	[24]
D	Dimension $100< d_{nom}<1000$	mm	Normal	$d_{nom}(1+0.003)$	$\frac{4+0.006d_{nom}}{d_{nom}(1+0.003)}$	[25]
D	Dimension $1000< d_{nom}< 2000$	mm	Normal	$d_{nom}+3$	$\frac{10}{d_{nom}+3}$	[25]
C_{0T}	Time-invariant component of the traffic load	-	Lognormal	9, 2.5*	0.1 * Mean	[28],[34]
T	Annual maxima of traffic load	kN/m^2	Gumbel	6.3, 1.75*	0.075 * Mean	[28],[34]
γ_w	Water density	kg/m^3	Det.	1200	-	[35]
C_D	Drag coefficient	-	Lognormal	0.7	0.25 * Mean	[24],[29]

*The characteristic traffic load values vary between notional lanes in accordance with Load Model 1 specified in the Eurocode [34].

Table 3. Input variables for probabilistic modeling of the pile-group ultimate bearing and lateral capacity.

Var.	Description	Unit	Dist.	Mean	Standard Deviation	Reference
$\Lambda^{(q_{pile-group})}$	Pile group efficiency factor under axial loading	-	Lognormal	1.3	0.21	[21]
$\Lambda^{(h_{pile-group})}$	Pile group efficiency factor under lateral loading	-	Lognormal	0.4	0.21	[21]
φ	Angle of internal friction	degree	Lognormal	35	0.15 * Mean	[36],[31]
Δ	Angle of interface friction	degree	-	0.8φ	-	[22]

Γ	Soil unit weight	$\mathrm{kN/m^3}$	Lognormal	20	0.1 * Mean	[22], [36]
k_o	Coefficient of lateral earth pressure	-	Det.	1	-	[22]

4 Results

The scour depth was estimated using Monte Carlo simulation by sampling from the input variables defined in Equations (1)–(6), thereby incorporating uncertainties within a probabilistic framework. This process produced a distribution of possible scour depths at the pier.

As no scour monitoring sensors were available for the studied case, and recognizing that such sensors often provide limited records that may not capture extreme flow events, synthetic observations were generated to represent scour depth measurements at Pier 1. These observations were used to update the scour depth correction factor.

The synthetic data were generated by first computing the deterministic scour depth and then sampling from the product of this value and the correction factor given in Table 1. This factor accounts for the bias between predicted and observed scour depths and was originally derived from a dataset of 515 field measurements, including both live-bed and clear-water scour conditions, by comparison with HEC-18 predictions [37].

To ensure that the generated samples reflect real scour depth, Kernel Density Estimation (KDE) was applied to approximate the probability density function of the sampled scour depths. Based on this estimated density, samples were probabilistically weighted, and resampling was performed such that values with higher likelihood were more frequently selected. This approach concentrates the synthetic observations around the most probable scour depths while preserving the inherent variability of the parameter.

The resulting observations were incorporated into the GBN to update the correction factor. The updated factor was subsequently used to estimate the scour depth at Pier 2. As shown in Figure 1, the posterior probability density function exhibits a reduced dispersion compared to the prior distribution, indicating a reduction in uncertainty following the update.

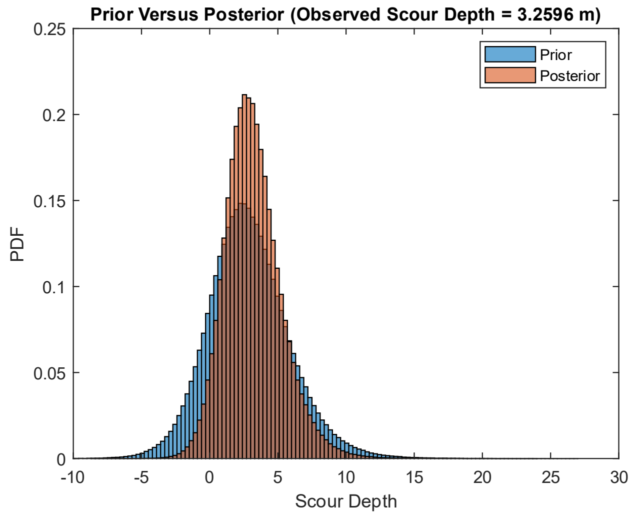

(a)

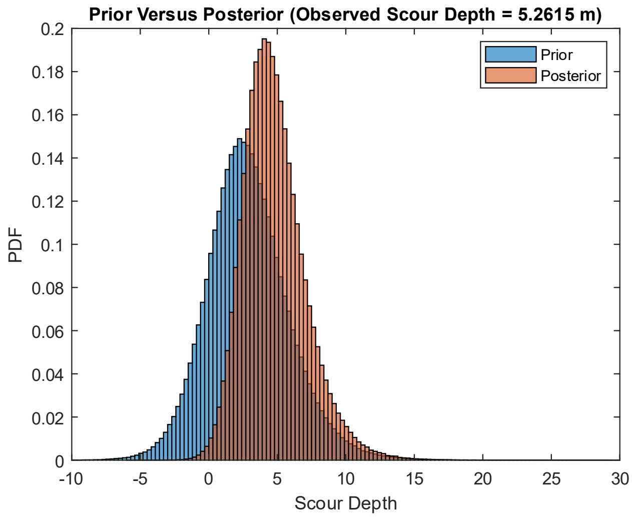

(b)

Figure 4. Prior and posterior PDFs of scour depth at Pier 33 under a discharge of 12,000 m^3/s: (a) posterior distribution obtained using an observed scour depth of 3.2596, and (b) posterior distribution obtained using an observed scour depth of 5.2615.

As illustrated in **Errore. L'origine riferimento non è stata trovata.**, the predicted scour depth extends into negative values, which is not physically realistic. This issue stems from the large standard deviation of the correction factor, which is nearly equal in magnitude to its bias. After updating the correction factor, the distribution shifts toward positive values, resulting in predictions that are more consistent with physical reality.

To enable a consistent comparison of system failure probabilities across a range of discharge levels, the structural reliability was assessed based on scour depth distributions derived without the inclusion of monitoring data. The analysis was first carried out at the level of individual piers for each failure mechanism. The overall probability of failure for each pier was then obtained by modeling the failure modes as a series system.

For the assessment of lateral capacity loss, the governing failure mechanism corresponds to the formation of two plastic hinges: one at the pile–pile cap connection and another along the embedded length of the pile within the soil. This mechanism is representative of deep pile behavior and is consistent with the present case study. According to [2], activation of alternative failure mechanisms associated with intermediate pile lengths would require scour depths on the order of 30 m, which is unrealistic.

Figure 5 illustrates the probability of failure of Pier 32 for the different failure mechanisms, along with the corresponding total failure probability of the pier. The results indicate that the probability of failure due to loss of lateral capacity of the pile group is significantly higher than that associated with loss of bearing capacity across all discharge levels. This observation is consistent with trends reported in the literature [7].

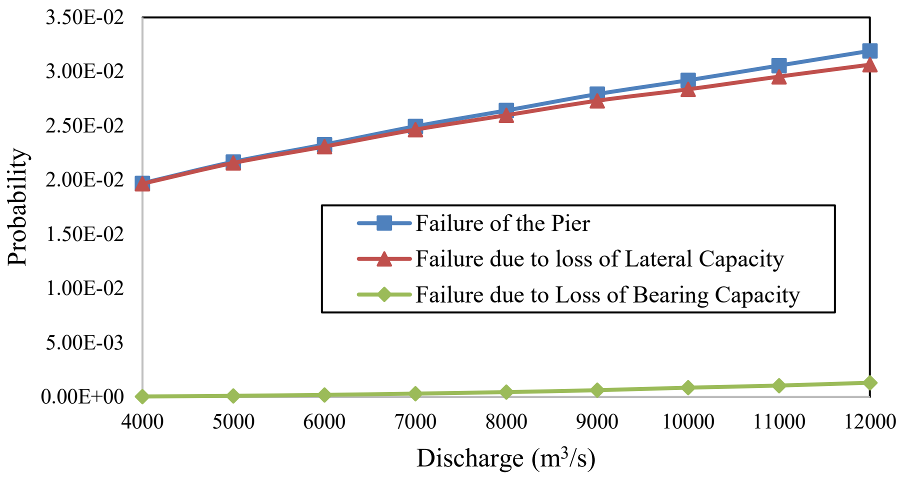

Figure 5. Probability of failure of Pier 32 across a range of discharges.

The reliability of a system comprising two identical piers arranged in series was then evaluated. The results are consistent with those obtained for a single pier, confirming that lateral capacity failure remains the dominant mechanism. To further investigate the primary drivers of this behavior, an additional scenario excluding scour effects was analyzed. Under this condition, the probability of failure due to loss of bearing capacity decreases substantially, approaching negligible values across all discharge levels. In contrast, only a minor reduction is observed in the probability of lateral failure.

As shown in Figure 6, differences between the two scenarios (with and without scour) are minimal at lower discharge levels. This is attributed to the limited development of scour under such conditions, which does not significantly affect structural capacity. Overall, these findings indicate that hydrodynamic forces associated with flooding, rather than scour, are the dominant contributor to system failure.

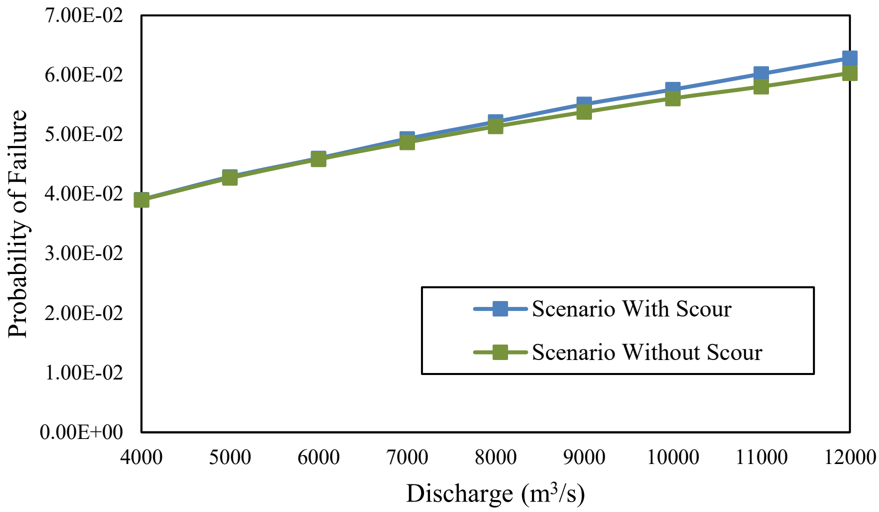

Figure 6. Probability of failure of the two-pier system over a range of discharge levels for scenarios with and without scour.

Although the results show that the loss of bearing capacity is not the governing failure mechanism, it still contributes to the overall failure probability of the system. The influence of traffic loading is presented in **Figure** *7*, where its contribution is shown to be non-negligible. This factor is particularly important in the context of risk assessment, as it directly affects consequence analysis and decision-making regarding bridge closure versus continued operation. In closure scenarios, the reliability corresponding to the no-traffic condition should be adopted for risk evaluation.

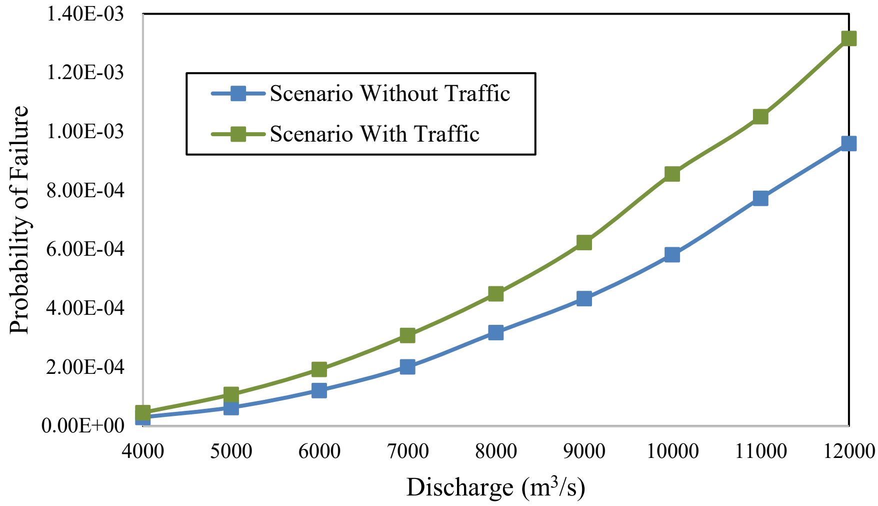

Figure 7. Probability of failure of Pier 32 across a range of discharge levels under two scenarios: with and without traffic.

5 Conclusion

This study presents a probabilistic framework for assessing the reliability of bridge piers subjected to flood-induced actions, with particular emphasis on the roles of scour and hydrodynamic loading. The methodology combines Monte Carlo simulation for probabilistic scour estimation with a Bayesian updating approach to incorporate scour observations. Structural reliability is evaluated considering two primary failure mechanisms: loss of bearing capacity and loss of lateral capacity of the pile group.

The results indicate that uncertainty in scour depth can be considerable, and the application of Bayesian updating is shown to effectively reduce this uncertainty and yield predictions that are more consistent with physical expectations.

From a structural reliability perspective, the analyses consistently indicate that failure due to loss of lateral capacity of the pile group governs the overall failure probability, both at the individual pier level and for the system of piers. In contrast, failure due to loss of bearing capacity plays a secondary role, although it still contributes to the total probability of failure. These findings are in agreement with observations reported in the literature.

The parametric investigation further reveals that hydrodynamic forces associated with flooding are the primary driver of failure, while the influence of scour is comparatively limited, particularly at lower discharge levels. The removal of scour effects leads to a significant reduction in the probability of bearing capacity failure, but only a minor change in lateral failure probability. This suggests that, for the studied case, the structural reliability is more sensitive to flow-induced forces than to foundation degradation caused by scour.

Overall, the proposed framework provides a comprehensive approach for integrating hydraulic, geotechnical, and structural uncertainties in bridge reliability assessment. While the study focuses on a representative pier, the results emphasize the importance of extending the analysis to all critical piers in river-crossing structures for a complete system-level evaluation.

Acknowledgments. A third level heading in 9-point font size at the end of the paper is used for general acknowledgments, for example: This study was funded by X (grant number Y).

Disclosure of Interests. It is now necessary to declare any competing interests or to specifically state that the authors have no competing interests. Please place the statement with a third level heading in 9-point font size beneath the (optional) acknowledgments, for example: The authors have no competing interests to declare that are relevant to the content of this article. Or: Author A has received research grants from Company W. Author B has received a speaker honorarium from Company X and owns stock in Company Y. Author C is a member of committee Z.

References

1. Zhu B, Frangopol DM. Risk-Based Approach for Optimum Maintenance of Bridges under Traffic and Earthquake Loads. J Struct Eng. 2013;139(3):422–34.
2. Ballio F, Ballio G, Franzetti S, Crotti G, Solari G. Actions monitoring as an alternative to structural rehabilitation: Case study of a river bridge. Struct Control Heal Monit. 2018;25(11):1–22.
3. Pizarro A, Manfreda S, Tubaldi E. The Science behind Scour at Bridge Foundations : A Review. Water. 2020;
4. Kellermann P, Schönberger C, Thieken AH. Large-scale application of the flood damage model RAilway Infrastructure Loss (RAIL). 2016;2357–71.
5. Transport-Cumbria Floods November 2009. 2009.
6. Tubaldi E, Macorini L, Izzuddin BA, Manes C, Laio F. A framework for probabilistic assessment of clear-water scour around bridge piers. Struct Saf. 2017;69:11–22.
7. Lin C, Han J, Bennett C, Parsons RL. Case History Analysis of Bridge Failures due to Scour. :204–16.
8. Argyroudis SA, Mitoulis SA. Vulnerability of bridges to individual and multiple hazards- floods and earthquakes. Reliab Eng Syst Saf. 2021;210(November 2020):107564.
9. Arneson LA, Zevenbergen LW, Lagasse PF, Clopper PE. Evaluating scour at bridges, Fifth Edition. 2012.
10. Sheppard DM, Melville B, Demir H. Evaluation of existing equations for local scour at bridge piers. 2013;
11. Yu P, Xu S, Chen J, Zhu L, Zhou J, Yu L, et al. Three-Dimensional Numerical Modeling of Local Scour Around Bridge Foundations Based on an Improved Wall Shear Stress Model. 2024;
12. Roulund A, Mutlu Sumer B, Fredsoe J, Michelsen J. Numerical and experimental investigation of flow and scour around a circular pile. 2005;534:351–401.
13. Hosseini R, Fazloula R, Saneie M, Amini A. Bagged Neural Network for Estimating

Scour Depth around Pile Groups. Intl J River Basin Manag. 2017;
14. Fosness RL, Schauer P V. Real-Time Pier Scour Monitoring and Observations at Three Scour-Critical Sites in Idaho , Water Years 2020 – 22. 2024.
15. Pizarro A, Tubaldi E. Quantification of modelling uncertainties in bridge scour risk assessment under multiple flood events. Geosciences. 2019;9(10).
16. Prendergast LJ., Gavin K. A review of bridge scour monitoring techniques. J Rock Mech Geotech Eng [Internet]. 2014;6(2):138–49. Available from: http://dx.doi.org/10.1016/j.jrmge.2014.01.007
17. Maroni A, Tubaldi E, Val DV., McDonald H, Zonta D. Using Bayesian networks for the assessment of underwater scour for road and railway bridges. Struct Heal Monit. 2021;20(5):2446–60.
18. Fadaei F, Francesco P, Maria G, Limongelli P. A Risk-based Framework for Scour Assessment and Emergency Management of Bridges. In 2025.
19. Hung CC, Yau WG. Behavior of scoured bridge piers subjected to flood-induced loads. Eng Struct [Internet]. 2014;80:241–50. Available from: http://dx.doi.org/10.1016/j.engstruct.2014.09.009
20. Lin C, Han J, Bennett C, Parsons RL. Analysis of Laterally Loaded Piles in Sand Considering Scour Hole Dimensions. J Geotech Geoenvironmental Eng. 2014;140(6):1–13.
21. Castro-Giraldo S, Friis T, Thöns S. DATA- AND SIMULATION-SUPPORTED SYSTEM RELIABILITY ASSESSMENT OF BRIDGES SUBJECTED TO EXTREME. 2025;1–12.
22. Giordano PF, Prendergast LJ., Limongelli MP. Quantifying the value of SHM information for bridges under flood-induced scour. Struct Infrastruct Eng. 2023;19(11):1616–32.
23. Tandjiria V, Teh CI, Low BK. Reliability analysis of laterally loaded piles using response surface methods. 2000;22.
24. Principles G. JCSS Probabilistic Model Code, Part 2: Load Models. 2001.
25. Reliability background of the Eurocodes. 2024.
26. Ghosn M, Moses F, Wang J. Design of Highway Bridges for Extreme Events. 2003.
27. Zorzi S, Broccardo M, Tonelli D, Zonta D. Reliability-based metrics for structural health monitoring information quality assessment. Struct Heal Monit. 2024;
28. Fib (International Federation for Structural Concrete). Partial factor methods for existing concrete structures. 2016.
29. Eurocode 1: Actions on structures - Part 1-6: General actions - Actions during execution. Vol. 1. 2011.
30. Bowles J. Foundation Analysis and Design. Civil Engineering Materials. 1996. 1143 p.
31. API RECOMMENDED PRACTICE 2A-WSD (RP 2A-WSD). Recommended Practice for Planning , Designing and Constructing Fixed Offshore Platforms — Working Stress Design. 2007.
32. Broms BB. Lateral Resistance of Piles in Cohesionless Soils. Soil Mech Found Div. 1964;
33. Marchi E, Roth G, Siccardi F. The november 1994 flood event on the po river: structural and non-structural measures against inundations. 1995;(November).
34. Eurocode 1: Actions on structures - Part 2: Traffic loads on bridges. Vol. 1. 2003.

35. Qeshta I, Hashemi M, Gravina RJ, Setunge S. Fragility analysis of non-ductile RC bridges subjected to extreme hydrodynamic force. In 2018. p. 1279–85.
36. Eijnden V Den. Reliability-based verification of limit states for geotechnical structures. 2024.
37. Johnson BPA. Comparison of Pier-Scour Equations Using Field Data. 1995;8(August):626–9.